

1 Development of a coupled current-wave model
2 to assess the impact of a hurricane on particle
3 transport

4 Thomas Dobbelaere, Emmanuel Hanert

5 February 9, 2021

6 **Abstract**

7 In most hydrodynamic model studies, currents and waves are simu-
8 lated separately. This is especially true for the simulation of passive
9 drifters, whose trajectories are often computed based solely on cur-
10 rents. Although this simplification holds for most situations, as the
11 force exerted by waves on currents can be neglected in fair weather
12 conditions, it may lead to significant errors in storm conditions, during
13 which local currents are strongly influenced by wind-generated waves.
14 In this study, current-wave interactions in heavy-wind conditions are
15 studied by coupling the unstructured-mesh hydrodynamic model SLIM
16 with the wave model SWAN in the Florida Reef Tract during Hurricane
17 Irma (Sep. 2017). This coupled model successfully reproduced both
18 the observed wave behavior and storm surge during the hurricane.
19 The modeled currents were then used to simulate the trajectories of
20 passive drifters during the passage of the hurricane. Our results show
21 that taking wave force into account induces variations of up 1 m/s
22 in modelled currents on the continental shelf break as well as in the
23 vicinity of reefs and islands. Wave-current interactions can therefore
24 strongly modify the transport of drifting material, such as sediments
25 and coral larvae, during heavy-wind events. That should in particular
26 affect connectivity modeling studies since coral mass spawning events
27 tend to occur during the hurricane season in the Caribbean.

²⁸ **1 Introduction**

²⁹ **2 Methods**

³⁰ **2.1 Wind and atmospheric pressure for Hurricane Irma**

³¹ In order to capture the wind speed profile of Irma in our model, high-
³² resolution H*Wind (Powell et al., 1998) wind fields were used. As these data
³³ represent 1-min averaged wind speeds, we multiplied them by a factor 0.93
³⁴ to obtain 10-min averaged wind speeds (Harper et al., 2010), more consist-
³⁵ ent with the time step of our model. Furthermore, H*Wind wind profiles
³⁶ did not cover the whole model extent during the hurricane and were thus
³⁷ blended within coarser wind field extracted from ECMWF ERA-5 datasets.
³⁸ Pressure fields of Irma were also constructed using ERA-5 data. However,
³⁹ the coarse resolution of the data set caused the depression at the center
⁴⁰ of the hurricane to get smoothed out, leading to an underestimation of the
⁴¹ pressure gradient in our model (see eq. 1). To better capture the central
⁴² depression of Irma, we built a hybrid pressure field using the position and the
⁴³ minimal pressure of the core of the hurricane based on its track in the HUR-
⁴⁴ DAT 2 database (Landsea and Franklin, 2013). Based on this information,
⁴⁵ the hybrid pressure field was constructed by combining an idealized Holland
⁴⁶ pressure profile (Lin and Chavas, 2012) within the radius of maximum wind
⁴⁷ speed of Irma (Knaff et al., 2018) with ERA-5 pressure field. The transition
⁴⁸ between from the Holland profile to ECMWF data outside the radius of
⁴⁹ maximum wind speed data was performed using a smooth step function.

⁵⁰ **2.2 Hydrodynamic model**

⁵¹ Ocean currents generated during hurricane Irma in the Florida Reef Tract
⁵² (FRT) were modelled using the unstructured-mesh depth-integrated coast
⁵³ ocean model SLIM ¹. The model mesh covers an area similar to the model
⁵⁴ extent of Dobbelaere et al. (2020b), that includes the FRT but also the
⁵⁵ Florida Strait and part of the Gulf of Mexico (Figure 1). However, this area
⁵⁶ has been slightly extended northeastward and westward in order to include

¹<https://www.slim-ocean.be>

57 the location of buoys for wave outputs validation. Furthermore, in order to
 58 withstand potential cell drying due to storm conditions in this study, we used
 59 the conservative mode of SLIM with wetting-drying, whose equations write:

$$\begin{aligned} \frac{\partial H}{\partial t} + \nabla \cdot (\mathbf{U}) &= 0 \\ \frac{\partial \mathbf{U}}{\partial t} + \nabla \cdot \left(\frac{\mathbf{U}\mathbf{U}}{H} \right) &= -f \mathbf{e}_z \times \mathbf{U} + \alpha g H \nabla(H - h) - \frac{1}{\rho} \nabla p_{\text{atm}} + \frac{1}{\rho} \boldsymbol{\tau}_s \quad (1) \\ &\quad + \nabla \cdot (\nu \nabla \mathbf{U}) - \frac{C_b}{H^2} |\mathbf{U}| \mathbf{U} + \gamma (\mathbf{U}_* - \mathbf{U}) \end{aligned}$$

60 where H is the water column height and \mathbf{U} is the depth-averaged transport;
 61 f is the Coriolis coefficient; g is the gravitational acceleration; h is the
 62 bathymetry; α is a coefficient stating whether the mesh element is wet
 63 ($\alpha = 1$) or dry ($\alpha = 0$); ν is the viscosity; C_b is the bottom drag coefficient;
 64 ∇p_{atm} is the atmospheric pressure gradient; $\boldsymbol{\tau}_s$ is the surface stress due
 65 to wind; and γ is a relaxation coefficient towards a reference transport \mathbf{U}_* .
 66 As in Frys et al. (2020) and Dobbelaere et al. (2020b), SLIM currents were
 67 relaxed towards HYCOM (Chassignet et al., 2007) in regions where the water
 68 depth exceeds a given threshold. At very high wind speeds, the white cap is
 69 blown off the crest of the waves, which generates a layer of droplets that acts
 70 as a slip layer for the winds at the ocean-atmosphere interface (Holthuijsen
 71 et al., 2012). This causes a saturation of the wind drag coefficient for strong
 72 winds (Donelan et al., 2004; Powell et al., 2003). To account for the impact
 73 of this saturation on the surface wind stress in our model, we implemented
 74 the wind drag parameterization of Moon et al. (2007).

75 The mesh resolution depended only on the distance to coastlines and reefs,
 76 bathymetry and bathymetry gradient in order to satisfy SWAN refinement
 77 criterion $h/A \geq a$, where h is the water depth and A is the element area.
 78 The mesh was generated using the Python library seamsh², based on the
 79 the open-source mesh generator GMSH (Geuzaine and Remacle, 2009) and
 80 is composed of approximately 7.7×10^5 elements. The coarsest elements,
 81 far away from the FRT, had a characteristic length size of about 5 km. Figure
 82 1 depicts how a 100-m spatial resolution mesh simulated fine-scale details
 83 of the ocean currents and significant wave height generated by hurricane
 84 Irma in the Florida Keys.

²<https://pypi.org/project/seamsh/>

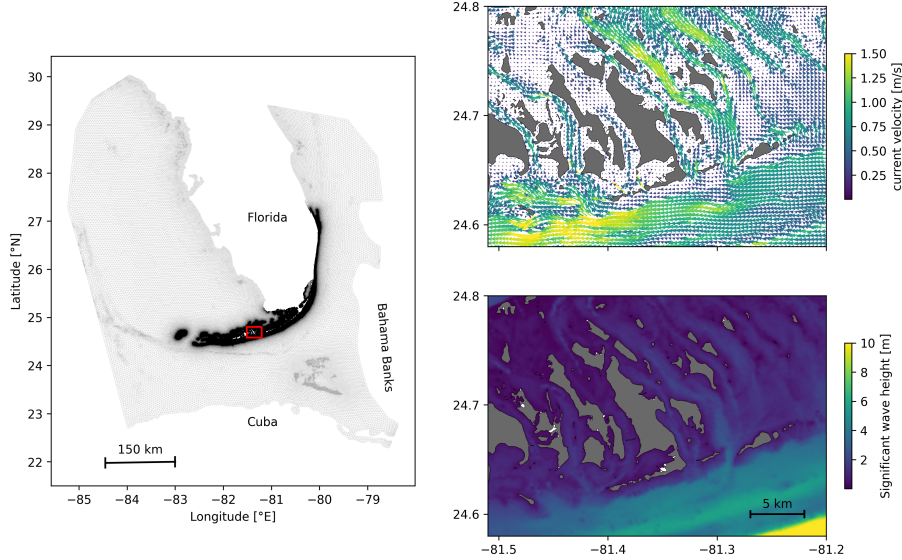


Fig. 1: Mesh of the computational domain with snapshots of simulated instantaneous currents and significant wave height on 2017-09-10 at 11:00:00. The mesh resolution ranges from 100 m in the Florida Keys to a maximum of 5 km offshore.

85 2.3 Wave model

86 Waves were modelled using parallel unstructured SWAN (Booij et al., 1999)
 87 on the same mesh as SLIM . This model solves the action balance equation,
 88 which reads (Mei, 1989):

$$\frac{\partial N}{\partial t} + \nabla_x \cdot [(c_g + \mathbf{u})N] + \frac{\partial}{\partial \theta}[c_\theta N] + \frac{\partial}{\partial \sigma}[c_\sigma N] = \frac{S_{in} + S_{ds} + S_{nl}}{\sigma} \quad (2)$$

89 where $N = E/\sigma$ is the wave action density; θ is the wave propagation direction;
 90 σ is the wave relative frequency; c_g is the wave group velocity, \mathbf{u} is SLIM
 91 depth-averaged current velocity; c_θ and c_σ are the propagation velocities in
 92 spectral space due to refraction and shifting in frequency due to variations
 93 in depth and currents; and S_{in} , S_{ds} , and S_{nl} respectively represent wave
 94 growth by wind, wave decay and nonlinear transfers of wave energy through
 95 interactions between triplets and quadruplets. Spectra were discretized with
 96 48 direction bins and 50 frequency bins logarithmically distributed from 0.3 to
 97 2 Hz. Exponential wind growth was parameterized using the formulation of
 98 Janssen (1991), while dissipations by whitecapping and bottom dissipations

99 followed the formulations of Komen et al. (1984) and Madsen et al. (1989)
 100 respectively. Coefficients for exponential wind growth and whitecapping
 101 parameterizations were based on the results of Siadatmousavi et al. (2011).
 102 Finally, wave boundary conditions were derived from WAVEWATCH III (Tol-
 103 man et al., 2009) spectral outputs at buoy locations. Depth-averaged Stokes
 104 drift was also computed by SWAN using the following formula:

$$\mathbf{u}_s = \int_0^{2\pi} \int_0^{+\infty} \frac{\sigma^3}{h \tanh(2kh)} E(\sigma, \theta) (\cos \theta, \sin(\theta)) d\sigma d\theta \quad (3)$$

105 where k is the norm of the wave vector; h is the water depth; and $E(\sigma, \theta)$ is
 106 the wave energy density.

107 2.4 Coupled model

108 The coupling between SLIM and SWAN is illustrated in Figure 2. The two
 109 models are run consecutively at each time step. First, SLIM computes the
 110 sea surface elevation η and depth-averaged current velocity $\mathbf{u} = (u, v)$.
 111 These quantities are transferred to SWAN to update the model water depth
 112 as well as the second term of equation 2 governing wave energy propagation
 113 in the geographic space. Moreover, in order for the two model to have con-
 114 sistent bottom dissipation parameterizations, SLIM bottom drag coefficient is
 115 transformed into a roughness length z_0 following the methodology of Dietrich
 116 et al. (2011). This roughness length is then converted into Madsen's bottom
 117 dissipation term in SWAN . SWAN then produces the wave-induced force on
 118 current τ_{wave} by computing the wave radiation stress gradient. This quantity
 119 is used to update the value of the surface stress τ_s in equation 1, that now
 120 becomes the sum of wind and wave-induced forces $\tau_s = \tau_{\text{wind}} + \tau_{\text{wave}}$.

121 2.5 Comparison of particle trajectories

122 To assess the impact of the wave coupling on the modelled currents during
 123 hurricane Irma, we compared the trajectories of virtual particles driven by
 124 currents produced by SLIM alone and SLIM +SWAN simulations in the Florida
 125 Keys. First, we identified the areas where the differences between the
 126 modelled currents were the largest. Then, we determined the potential

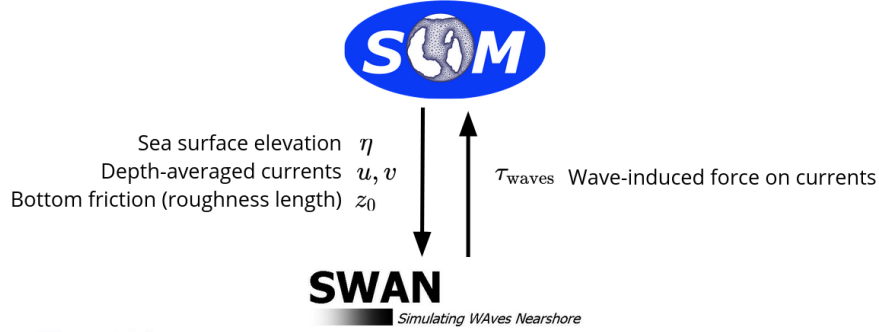


Fig. 2: Schematic illustration of the coupled SLIM +SWAN model.

127 origination regions of particles reaching these areas on the passage of the
 128 hurricane through the Florida Keys using backtracking methods (Dobbelaeere
 129 et al., 2020a). These regions are highlighted by the 4 release regions of
 130 Fig. 7. Finally, particles were released from these four regions and advected
 131 by currents produced by the coupled and uncoupled models. At each time
 132 step, the center of mass of the modelled particle clouds were computed.
 133 The distance between these centers of mass was used as a measure of the
 134 impact of the wind-generated wave coupling on the modelled current in the
 135 Florida Keys during hurricane Irma.

136 **3 Results**

137 **3.1 Validation**

138 Comparisons of the H*Wind wind and hybrid pressure fields with station
 139 measurements at Vaca Key are shown in Fig. 3. The observed pressure
 140 at the station is well reproduced by the reconstructed hybrid pressure field.
 141 H*Wind profile agree well with field measurements as well despite a slight
 142 overestimation of the peak wind speed.

143 **QUESTION: Should I use quantitative results such as RMSE ?**

144 To validate the hydrodynamic outputs of the coupled wave-current model,
 145 the computed sea surface elevation was compared with tide gauge measure-
 146 ments on the Eastern and Western coasts of Florida as well as in the Florida
 147 Keys. Figure 4 shows a good fit between simulated and measured elevation

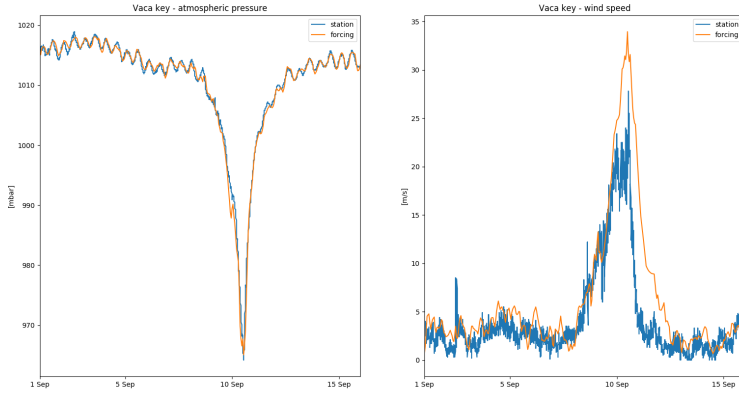


Fig. 3: The atmospheric forcings have been validated with meteorological station observations at Vaca Key. The reconstructed atmospheric pressure and wind speed agree well with field measurements.

148 at all stations, where the model succeeds in reproducing the observed tide
 149 surge caused by the passage of the Irma. Modelled currents were validated
 150 against ADCP data at moorings C10, C12 and C13, respectively located at
 151 the 25, 50, and 50 m isobaths of the inner Florida shelf (Liu et al., 2020).
 152 Measured and modelled depth-averaged currents at station C10 are shown
 153 in Fig. 4. The current speed and direction during the hurricane agree well
 154 with observations.

155 The wave parameters computed by the coupled model were validated
 156 against field measurements as well. Validation data was extracted from four
 157 buoys, two in the Eastern coast Florida and two in the inner shelf. Results
 158 of Fig. 5 show that the model reproduces correctly the timing and ampli-
 159 tude of the significant wave height peak during the hurricane for all four
 160 stations. Modelled wave period and direction are in good agreement with
 161 measurement as well, as shown for station 42036.

162 3.2 Impact of waves

163 4 Discussion and conclusions

164 Impact of waves on coral connectivity

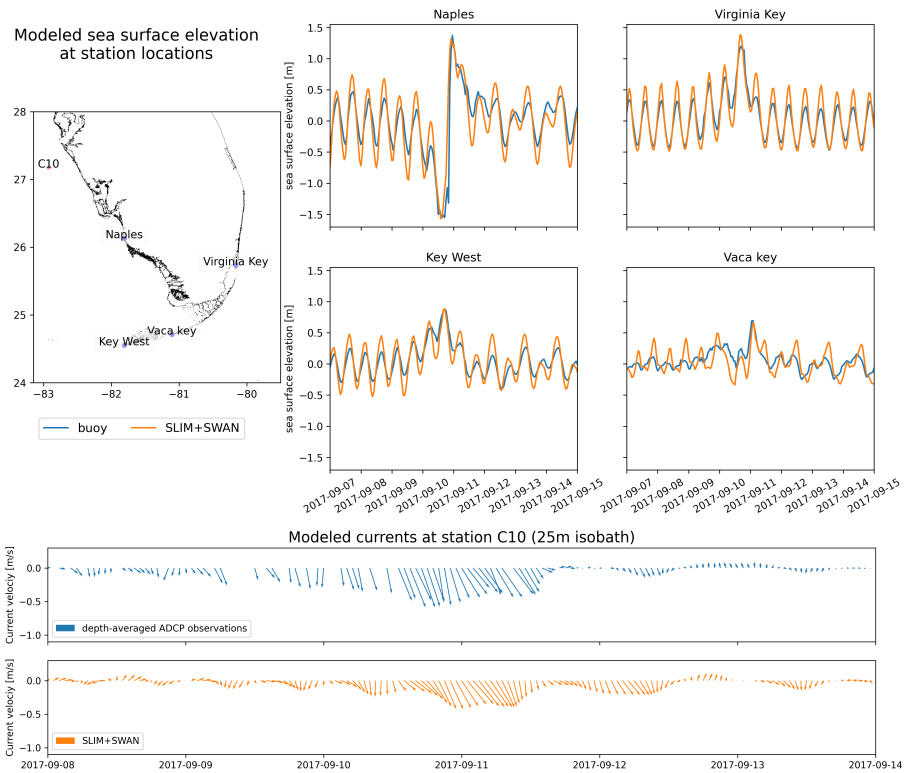


Fig. 4: The sea-surface elevation produced by the coupled wave-current model agrees with SSE and current velocity observations at different stations. The fit is particularly good in the Florida Keys and in Naples, on the inner Florida shelf. The coupled model currents have been validated against current meter data on the inner Florida shelf. The current speed and direction during the hurricane agrees well with the observations.

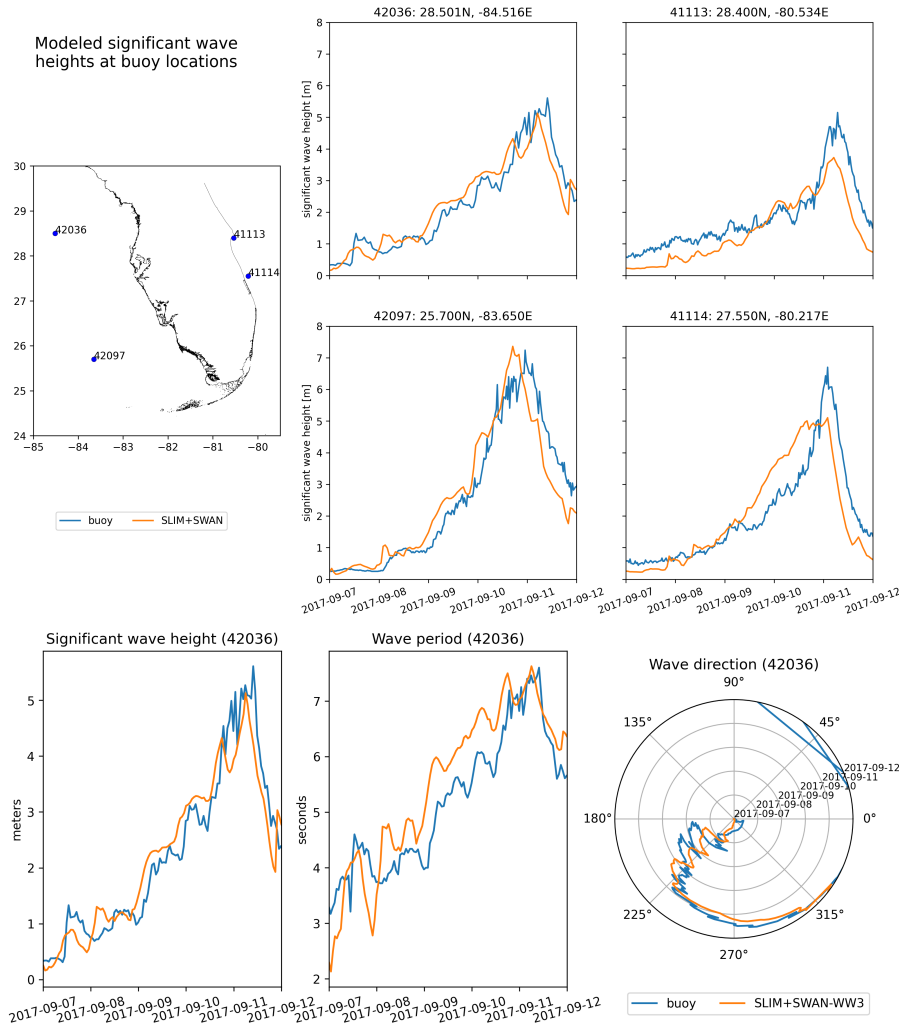


Fig. 5: The significant wave height produced by the coupled model has been compared to buoy measurements at 4 different stations. The timing and amplitude of the peak during the hurricane is correctly reproduced for all stations. For station 42036, the period and direction of the waves also agree well with observations

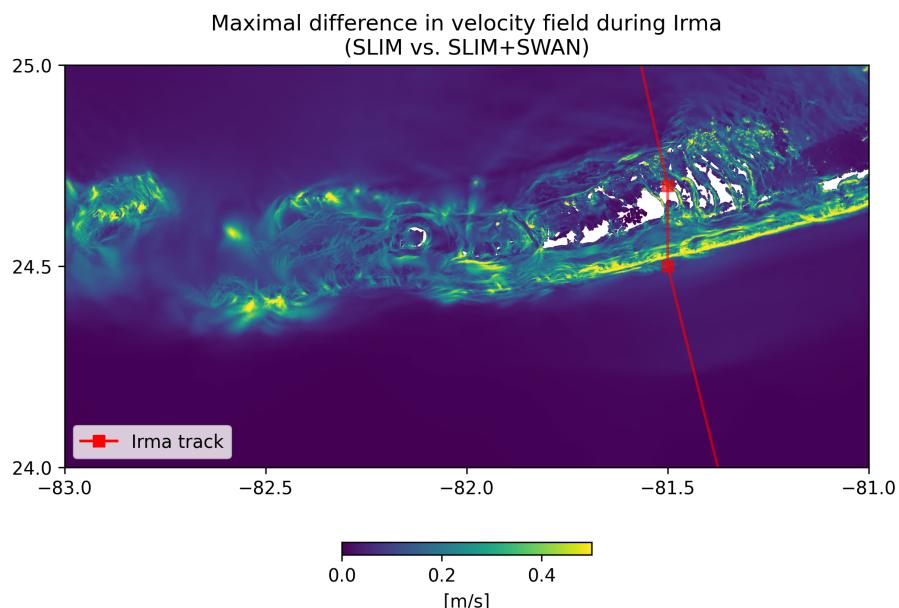


Fig. 6: Maximum of the difference between SLIM and SLIM+SWAN currents speed between 2017-09-07 00:00:00 and 2017-09-13 00:00:00. The difference between the coupled and uncoupled model, which represents the effect of the wave-induced stress, can yield differences of 0.5 m/s in the simulated currents during the passage of the hurricane. SLIM+SWAN currents velocities are larger than the currents modeled by SLIM alone.

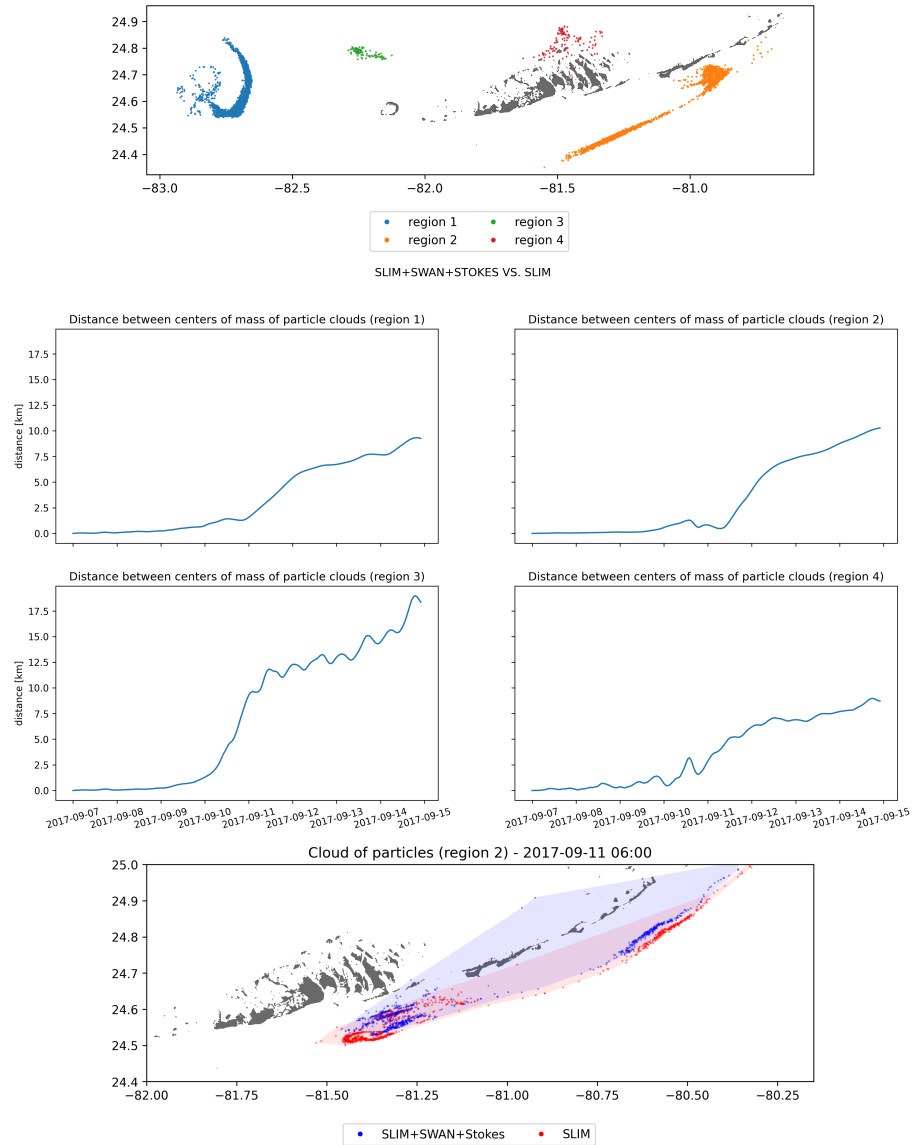


Fig. 7: Comparison of passive drifters trajectories with SLIM+SWAN+Stokes drift vs. SLIM alone. A snapshot of the positions of the particles released from region 2 is shown after the passage of Irma in the Florida Keys. Particles advected by the currents of the coupled model tend to remain on the shelf while particles advected by SLIM alone are mostly transported along the shelf break

¹⁶⁵ Ability of wave model to correctly capture gradient in significant wave height
¹⁶⁶ due to current-waves interactions under tropical cyclones depends on:

- ¹⁶⁷ • Spatial (10km → 5km) and spectral (36 dir. → 48 dir.) resolution
¹⁶⁸ (Hegermiller et al., 2019)
- ¹⁶⁹ • Directional spreading of incident waves (Villas Bôas et al., 2020)

¹⁷⁰ **Conflict of Interest Statement**

¹⁷¹ The authors declare that the research was conducted in the absence of any
¹⁷² commercial or financial relationships that could be construed as a potential
¹⁷³ conflict of interest.

¹⁷⁴ **Author Contributions**

¹⁷⁵ **Funding**

¹⁷⁶ **Acknowledgments**

¹⁷⁷ Computational resources were provided by the Consortium des Équipements
¹⁷⁸ de Calcul Intensif (CÉCI), funded by the F.R.S.-FNRS under Grant No. 2.5020.11.
¹⁷⁹ Thomas Dobbelaere is a PhD student supported by the Fund for Research
¹⁸⁰ training in Industry and Agriculture (FRIA/FNRS).

¹⁸¹ **Supplementary Material**

¹⁸² The Supplementary Material for this article is attached to the submitted
¹⁸³ document.

¹⁸⁴ **References**

- ¹⁸⁵ Booij, N., Ris, R. C., and Holthuijsen, L. H. (1999). A third-generation wave
¹⁸⁶ model for coastal regions: 1. Model description and validation. *Journal*
¹⁸⁷ *of geophysical research: Oceans*, 104(C4):7649–7666.
- ¹⁸⁸ Chassignet, E. P., Hurlbert, H. E., Smedstad, O. M., Halliwell, G. R., Hogan,
¹⁸⁹ P. J., Wallcraft, A. J., Baraille, R., and Bleck, R. (2007). The HYCOM
¹⁹⁰ (hybrid coordinate ocean model) data assimilative system. *Journal of*
¹⁹¹ *Marine Systems*, 65(1-4):60–83.
- ¹⁹² Dietrich, J., Westerink, J., Kennedy, A., Smith, J., Jensen, R., Zijlema, M.,
¹⁹³ Holthuijsen, L., Dawson, C., Luettich, R., Powell, M., et al. (2011).
¹⁹⁴ Hurricane gustav (2008) waves and storm surge: Hindcast, synoptic
¹⁹⁵ analysis, and validation in southern Louisiana. *Monthly Weather Review*,
¹⁹⁶ 139(8):2488–2522.
- ¹⁹⁷ Dobbelaere, T., Muller, E., Gramer, L., Holstein, D., and Hanert, E. (2020a).
¹⁹⁸ Report on the potential origin of the SCTLD in the Florida Reef Tract.
¹⁹⁹ Available online at: <https://floridadep.gov/rcp/coral/documents/report-potential-origin-sctld-florida-reef-tract>.
- ²⁰¹ Dobbelaere, T., Muller, E. M., Gramer, L. J., Holstein, D. M., and Hanert, E.
²⁰² (2020b). Coupled epidemic-hydrodynamic modeling to understand the
²⁰³ spread of a deadly coral disease in Florida. *Frontiers in Marine Science*,
²⁰⁴ 7:1016.
- ²⁰⁵ Donelan, M., Haus, B., Reul, N., Plant, W., Stiassnie, M., Gruber, H., Brown,
²⁰⁶ O., and Saltzman, E. (2004). On the limiting aerodynamic roughness of
²⁰⁷ the ocean in very strong winds. *Geophysical Research Letters*, 31(18).
- ²⁰⁸ Frys, C., Saint-Amand, A., Le Hénaff, M., Figueiredo, J., Kuba, A., Walker, B.,
²⁰⁹ Lambrechts, J., Vallaeyns, V., Vincent, D., and Hanert, E. (2020). Fine-
²¹⁰ scale coral connectivity pathways in the Florida Reef Tract: implications
²¹¹ for conservation and restoration. *Frontiers in Marine Science*, 7:312.
- ²¹² Geuzaine, C. and Remacle, J.-F. (2009). Gmsh: A 3-d finite element mesh
²¹³ generator with built-in pre-and post-processing facilities. *International*
²¹⁴ *journal for numerical methods in engineering*, 79(11):1309–1331.

- 215 Harper, B., Kepert, J., and Ginger, J. (2010). *Guidelines for converting*
216 *between various wind averaging periods in tropical cyclone conditions.*
217 Citeseer.
- 218 Hegermiller, C. A., Warner, J. C., Olabarrieta, M., and Sherwood, C. R.
219 (2019). Wave-current interaction between Hurricane Matthew wave
220 fields and the Gulf Stream. *Journal of Physical Oceanography*,
221 49(11):2883–2900.
- 222 Holthuijsen, L. H., Powell, M. D., and Pietrzak, J. D. (2012). Wind and waves
223 in extreme hurricanes. *Journal of Geophysical Research: Oceans*,
224 117(C9).
- 225 Janssen, P. A. (1991). Quasi-linear theory of wind-wave generation applied
226 to wave forecasting. *Journal of physical oceanography*, 21(11):1631–
227 1642.
- 228 Knaff, J. A., Sampson, C. R., and Musgrave, K. D. (2018). Statistical tropi-
229 cal cyclone wind radii prediction using climatology and persistence:
230 Updates for the western North Pacific. *Weather and Forecasting*,
231 33(4):1093–1098.
- 232 Komen, G., Hasselmann, S., and Hasselmann, K. (1984). On the exis-
233 tence of a fully developed wind-sea spectrum. *Journal of physical*
234 *oceanography*, 14(8):1271–1285.
- 235 Landsea, C. W. and Franklin, J. L. (2013). Atlantic hurricane database un-
236 certainty and presentation of a new database format. *Monthly Weather*
237 *Review*, 141(10):3576–3592.
- 238 Lin, N. and Chavas, D. (2012). On hurricane parametric wind and appli-
239 cations in storm surge modeling. *Journal of Geophysical Research:*
240 *Atmospheres*, 117(D9).
- 241 Liu, Y., Weisberg, R. H., and Zheng, L. (2020). Impacts of hurricane Irma
242 on the circulation and transport in Florida Bay and the Charlotte Harbor
243 estuary. *Estuaries and Coasts*, 43(5):1194–1216.
- 244 Madsen, O. S., Poon, Y.-K., and Gruber, H. C. (1989). Spectral wave
245 attenuation by bottom friction: Theory. In *Coastal Engineering 1988*,
246 pages 492–504.

- 247 Mei, C. C. (1989). *The applied dynamics of ocean surface waves*, volume 1.
248 World scientific.
- 249 Moon, I.-J., Ginis, I., Hara, T., and Thomas, B. (2007). A physics-based
250 parameterization of air–sea momentum flux at high wind speeds and
251 its impact on hurricane intensity predictions. *Monthly weather review*,
252 135(8):2869–2878.
- 253 Powell, M. D., Houston, S. H., Amat, L. R., and Morisseau-Leroy, N. (1998).
254 The HRD real-time hurricane wind analysis system. *Journal of Wind
255 Engineering and Industrial Aerodynamics*, 77:53–64.
- 256 Powell, M. D., Vickery, P. J., and Reinhold, T. A. (2003). Reduced drag coeffi-
257 cient for high wind speeds in tropical cyclones. *Nature*, 422(6929):279–
258 283.
- 259 Siadatmousavi, S. M., Jose, F., and Stone, G. (2011). Evaluation of two WAM
260 white capping parameterizations using parallel unstructured SWAN
261 with application to the Northern Gulf of Mexico, USA. *Applied Ocean
262 Research*, 33(1):23–30.
- 263 Tolman, H. L. et al. (2009). User manual and system documentation of
264 WAVEWATCH III TM version 3.14. *Technical note, MMAB Contribution*,
265 276:220.
- 266 Villas Bôas, A. B., Cornuelle, B. D., Mazloff, M. R., Gille, S. T., and Arduin,
267 F. (2020). Wave–current interactions at meso-and submesoscales:
268 Insights from idealized numerical simulations. *Journal of Physical
269 Oceanography*, 50(12):3483–3500.